Bio-Inspired Vapor-Responsive Colloidal Photonic Crystal Patterns by Inkjet Printing

Ling Bai,[†] Zhuoying Xie,[*,†,‡] Wei Wang,[†] Chunwei Yuan,[*,†] Yuanjin Zhao,[†] Zhongde Mu,[†] Qifeng Zhong,[†] and Zhongze Gu[*,†,‡]

[†]State Key Laboratory of Bioelectronics, School of Biological Science and Medical Engineering, Southeast University, Nanjing 210096, China and [‡]Suzhou Key Laboratory of Environment and Biosafety, Research Institute of Southeast University in Suzhou, Suzhou 215123, China

ABSTRACT Facile, fast, and cost-effective technology for patterning of responsive colloidal photonic crystals (CPCs) is of great importance for their practical applications. In this report, we develop a kind of responsive CPC patterns with multicolor shifting properties by inkjet printing mesoporous colloidal nanoparticle ink on both rigid and soft substrates. By adjusting the size and mesopores' proportion of nanoparticles, we can precisely control the original color and vapor-responsive color shift extent of mesoporous CPC. As a consequence, multicolor mesoporous CPCs patterns with complex vapor responsive color shifts or vapor-revealed implicit images are subsequently achieved. The complicated and reversible multicolor shifts of mesoporous CPC patterns are favorable for immediate recognition by naked eyes but hard to copy. This approach is favorable for integration of responsive CPCs with controllable responsive optical properties. Therefore, it is of great promise for developing advanced responsive CPC devices such as anticounterfeiting devices, multifunctional microchips, sensor arrays, or dynamic displays.

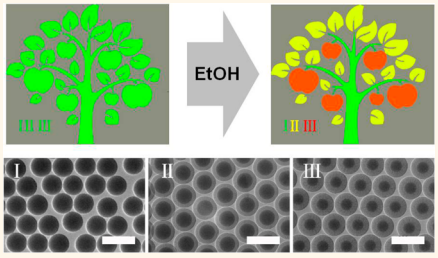

KEYWORDS: mesoporous silica nanoparticles · vapor responsive · colloidal photonic crystals · inkjet printing · pattern

Responsive colloidal photonic crystals (CPCs) have drawn great consideration, due to their strong capability to control and manipulate the light propagation with tunability[1−3] and promising applications in displays,[4−7] sensors,[8−14] lasers,[15] and anticounterfeiting trademarks.[16−19] For these applications, effective and high resolution patterning technology for responsive CPCs was of great importance. In the past decades, a variety of CPC patterning strategies have been proposed, such as lithographic patterning by UV/vis polymerization,[20,21] microcontact printing,[22,23] photonic paper/inks,[24−26] and so on.[11,27] However, it is still a challenge to pattern responsive CPCs with distinct color shifting properties by facile, fast, and cost-effective methods.

Recently, as a precise, versatile, low-cost and waste eliminated patterning method,[28−33] inkjet printing method has already been exploited for the preparation of CPC devices.[12,34−36] It allows flexible design of printing images, inks and substrates and favors the control of the shapes,[37,38] aligns,[39,40] and special optical properties of CPCs.[41,42] But in order to achieve complex responsive CPC patterns, specific CPC inks that could respond to external stimulus as well as specific substrates are required. Here, inspired by *Tmesisternus isabellae*, we proposed a novel kind of CPC patterns with vapor-revealed implicit images by inkjet printing mesoporous colloidal nanoparticle ink on both rigid and soft substrates. *T. isabellae* are one kind of longhorn beetles, who can reversibly switch their color from gold to red according to the humidity changes of surrounding environment.[43] The color shift is caused by the adsorption of water vapor in their elytra, which leads to the changes of thickness and average refractive index of their multilayered scales. Imitating its mechanism allows one to compose the vapor-responsive CPCs presented here by mesoporous silica naoparticles (MSNs). These MSNs own large surface area and strong vapor adsorption capabilities.[44,45] Thus, the mesoporous CPC (MCPC) composed of MSNs favored the capillary condensation process of vapor in their hierarchical porous structure, which

* Address correspondence to gu@seu.edu.cn, zyxie@seu.edu.cn, cwy@seu.edu.cn.

Received for review August 19, 2014 and accepted October 9, 2014.

Published online October 09, 2014
10.1021/nn504659p

promoted the increase of their refractive index and led to their color shifts.[46−51] And when the size and mesopores' proportion of mesoporous nanoparticles in the ink were adjusted, the original color and vapor-responsive color shift extent of MCPC was precisely controlled. As a consequence, multicolor responsive CPC patterns with complex vapor-responsive color shifting features or implicit images were achieved. The flexibly designed multicolor shifting properties of MCPC patterns were reversible and repeatable and their implicit image revealed by vapors was of high concealment, and thus, they were favorable for anti-counterfeiting applications. This approach showed great potential for fabrication of complex responsive CPC patterns with multiple color shifting responsive properties, which is of great importance for developing miniaturized or multifunctional responsive CPC devices, such as anticounterfeiting devices, multifunctional microchips, sensor arrays, and dynamic displays.

RESULTS AND DISCUSSION

A typical printing process of a responsive CPC pattern was illustrated in Figure 1a. Latex droplets of MSNs or solid silica nanoparticles (SSNs) were inkjet printed onto a substrate with designed pattern. Then, the nanoparticles spontaneously assembled into well-ordered CPC domes during drying procedure (see Figure 1b). By the integration of different MCPCs or CPCs with same origin color but distinct responsive color shift extent to the pattern, implicit image was flexibly designed. The hidden information was revealed by exposure to certain vapors, as shown in Figure 1c. Therefore, this method provided a high quality of concealment and was favorable for anti-counterfeiting and dynamic display applications.

Dual-Color Responsive CPC Pattern with Implicit Image. A dual-color responsive CPC pattern in N_2 was first prepared, and its optical image in N_2 was shown in Figure 2a. In this pattern, the tree leaves were composed of MCPCs and the tree trunk was made of solid SiO_2 CPCs (SCPCs). Two parts displayed same green color in N_2, which was difficult to distinguish from each other, so that the image of tree leaves composed of MCPCs was hidden. However, when the pattern was exposed to special vapors like ethanol (EtOH), the MCPC part displayed obvious color change; meanwhile, the color of SCPC part changed little, so that the implicit image of the pattern was revealed, as seen in Figure 2b. Microscope images of MCPC and SCPC microdots in N_2 were separately shown in Figure 2c,d. Both MCPC and SCPC microdots displayed bright green color. And they were both of high uniformity and orderly arrangements, contributing to the consistent color of the pattern. The SEM images showed an ordered arrangement of colloidal nanoparticles in CPC microdots, which contributed to the bright color and shape reflection peaks of the responsive CPC pattern

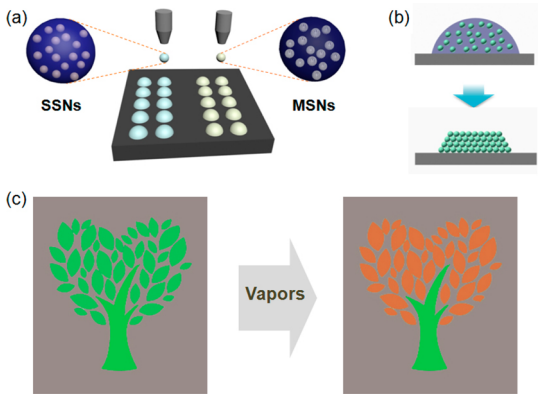

Figure 1. (a) Illustration for the inkjet printing process of the MCPC pattern. (b) The nanoparticles self-assembled into well-ordered structures during the drying procedure. (c) Designed implicit image of MCPC pattern revealed by certain vapor.

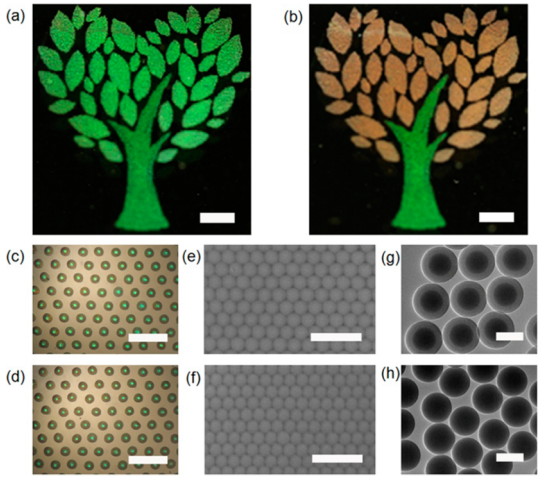

Figure 2. (a and b) Color changes of the printed pattern in N_2 and saturated EtOH atmosphere, scale bar: 0.5 cm. (c and d) Optical microscopy image of the printed MCPC and SCPC microdots, scale bar: 200 μm. (e and f) Top-view SEM images of MCPC microdots and SCPC microdots, scale bar: 1 μm. (g and h) TEM images of MSNs and SSNs, scale bar: 200 nm.

(Figure 2e,f). For a better understanding of the three-dimensional structure of the MCPC microdot, the cross section of a MCPC microdot was investigated, as shown in Supporting Information Figure S1. SEM images showed that MSNs were mainly in a face-centered cubic arrangement in MCPC microdots, which favored calculation and design of their responsive optical properties. The contrasting vapor responsive color-shifting properties of SCPCs and MCPCs were due to the difference of two kinds of colloidal nanoparticles. As shown in Figure 2g, the MSNs were composed of uniform solid cores and mesoporous shells. Their perpendicular mesoporous channels were favorable for vapor condensation in the pores and resulted in the great increase of refraction index, which thus led to remarkable color changes. But this feature was not possessed by SSNs, as they did not have mesostructures (see Figure 2h).

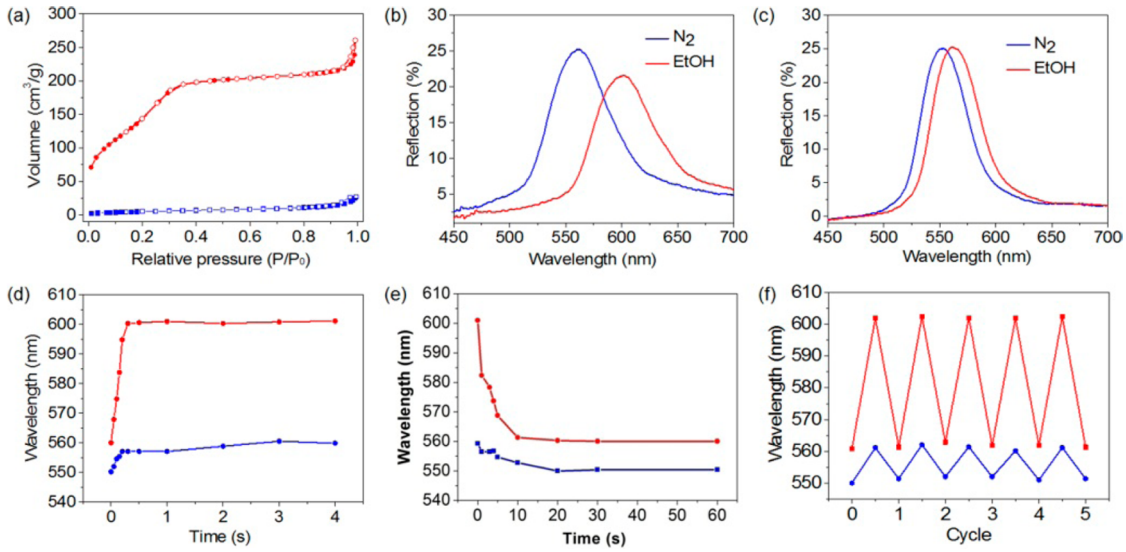

Figure 3. (a) The nitrogen adsorption/desorption isotherms of MSNs and SSNs, blue squares represent for SSNs and red circles represent for MSNs. (b) Reflection spectra of the MCPCs in N_2 and EtOH vapors. (c) Reflection spectra of the SCPCs in N_2 and EtOH vapors. (d) Time-dependent Bragg diffraction peak positions of MCPCs and SCPCs after exposure to EtOH vapors. (e) Time-dependent Bragg diffraction peak positions of MCPCs and SCPCs after exposure to N_2 vapors. (f) Reversible PBG movements of MCPCs and SCPCs by alternately exposing to N_2 and saturated EtOH vapor. (d–f) Blue circles represent for SSNs and red circles represent for MSNs.

Responsive Properties of the Dual-Color CPC Pattern. To exhaustively investigate the vapor-responsive property of the pattern for practical applications, their vapor adsorption abilities, color-shifting features, responding speed and durability were subsequently studied. The nitrogen adsorption/desorption experiments were performed to characterize the vapor adsorption abilities of MSNs and SSNs, as shown in Figure 3a. The surface area and pore volume of MSNs were much larger than those of SSNs; thus, they provided more absorbing sites and spaces for vapor condensation in MCPCs. As shown in Figure 3b,c, the reflection peak of the MCPCs shifted 39 nm on exposure to saturated EtOH vapor, and which of the SCPCs only shifted 7 nm. The nitrogen adsorption/desorption and spectral results demonstrated that large surface area and high pore volume rate of MSNs were responsible for obvious color shifts of MCPCs. We also investigated the responsive ability of MCPCs to other vapors, as shown in Supporting Information Figure S2. The results suggested that MCPCs could also respond to other vapors, but responsive color shifting contents were distinct. The vapor responding speed of the pattern was subsequently investigated. As plotted in Figure 3d, the reflection peak position of MCPCs began to change as soon as they were exposed to EtOH vapor. In addition, it red-shifted 30 nm in the first 0.2 s and reached its equilibrium after only 0.5 s. In the meantime, the reflection peak of SCPCs shifted slightly. The rapid vapor responsive property of MCPCs was extremely favorable for immediate recognition by naked eyes as well as optical devices; thereby, they possess a potential as security feature for anticounterfeiting authentications. The recovery speed of the pattern on exposure to N_2 was also shown in Figure 3e. Reflection peaks of MCPCs and SCPCs both got back to its origin position after less than 1 min, which did not affect their potential security utilizations. The reproduction of the responsive properties of pattern was subsequently investigated by alternately exposing to N_2 and saturated EtOH vapors for several cycles. The first five cycles were plotted in Figure 3f, and it was clear that the conversion of peak positions to N_2 and saturated EtOH vapor was reversible and repeatable. In addition, their color transitions were based on the physical structural changes; thus, they are free from photobleaching and durable. So the MCPC pattern owned a fast vapor responsive speed and a good recovery capability and, thus, was of great promise for practical anticounterfeiting authentications.

Control of Responsive Optical Properties of MCPCs. For achievement of complex multicolor MCPC patterns with complex vapor-responsive properties, integration of different responsive MCPCs with precisely controlled original color and responsive color shifts was needed. With controllable synthesis of MSNs with different size and mesopores' proportion, we successfully fabricated multicolor MCPC patterns with designed color-shifting properties. A series of MSNs with same solid core but different mesoporous shell thicknesses (see Supporting Information Figure S3) were synthesized first to control the colors of the MCPCs, as shown in Figure 4a–f. The colors of MCPC films prepared by these MSNs changed from violet to red when mesoporous shells thicknesses increased (see Supporting Information Figure S4). Furthermore, by controlling solid core and mesoporous shell thicknesses of MSNs at the same time,

we obtained MCPCs with same colors but different vapor-responsive color shifting properties. As shown in Supporting Information Figure S5a−c, the CPC films prepared by SSNs and two MNSs with designed core/shell sizes (shown in Figure 4g−i) displayed the same color in N_2. However, due to their distinct surface area and pore volume (Supporting Information Figure S6), the corresponding CPC films displayed distinct color shifts in EtOH vapor (Supporting Information Figure S5d−f). The color shift mechanism can be expressed by Bragg's law under normal incidence (eq 1),

$$\lambda = 1.633d\sqrt{f_{void}n_{void}^2 + f_{core}n_{SiO2}^2 + f_{mpore}n_{mpore}^2 + f_{mSiO2}n_{SiO2}^2} \quad (1)$$

where λ is the peak wavelength of the MCPCs; d is the diameter of MSNs; f_{void}, f_{core}, f_{mSiO2}, and f_{mpore} represent the volume rate of void space, SiO_2 core in MSNs, SiO_2 in mesoporous shells, and mesopores in mesoporous shells, respectively. The parameters n_{void}, n_{SiO2}, and n_{mpore} represent the refractive index of air, SiO_2, and mesopores, respectively. In particular, the values of n_{mpore} changed in different vapor atmospheres, which was responsible for the vapor-responsive color shifting properties of MCPCs. When MCPCs were placed in N_2, mesopores were filled with N_2 vapor, so value of n_{mpore} was 1, the same as n_{N2}. However, when MCPCs were placed in EtOH vapor, capillary condensed EtOH solutions filled up with the mesopores, so value of n_{mpore} was estimated to be 1.36 (n_{EtOH} = 1.36). In eq 1, the values of n_{void}, n_{SiO2}, and f_{void} were known to be 1, 1.46, and 0.74 respectively. The value of f_{core} was calculated by measuring core/shell rates of MSNs in TEM figures, and the empirical value of f_{mpore} was 0.55, which was calculated by measuring λ of MCPCs in N_2. So eq 1 can be reduced into Eq2.

$$\lambda = 1.633d\sqrt{0.97 + 0.87f_{core} + 0.41(1 - f_{core})n_{mpore}^2} \quad (2)$$

According to this formula, MSNs of same core but thicker mesoporous shell or same diameter but higher mesoporous rate can lead to larger Bragg diffraction shifts of MCPCs they composed. In this way, color and vapor-chromic properties of MCPCs can be precisely calculated and designed. As shown in Supporting Information Figure S7, the experimental data of the reflection peaks of fabricated MCPCs in N_2 or EtOH vapor were in accordance with the calculated curves from eq 2.

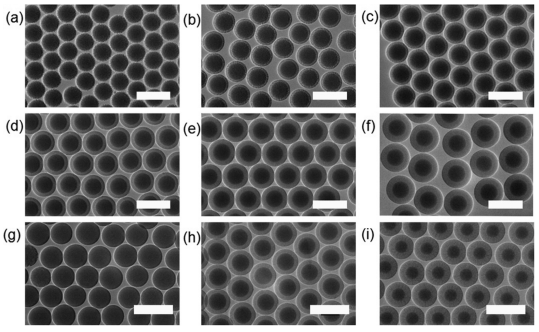

Figure 4. (a−f) TEM images of synthesized MSNs growing on the same SiO_2 seeds, scale bar: 350 nm. (g−i) TEM images of synthesized MSNs and SSNs for controlling the vapor-chromic features of MCPC patterns, scale bar: 400 nm.

Complex Responsive CPC Patterns with Vapor-Revealed Implicit Images. On the basis of the precisely controlled monodisperse MSNs, multicolor MCPC patterns with more complex responsive color shifting properties were then demonstrated. As shown in Figure 5a, a responsive CPC pattern with complex vapor-revealed implicit images was prepared. The pattern was composed of three kinds of CPCs, which displayed same color in N_2 but different vapor-responsive color shifting properties. When it was placed in EtOH vapor atmosphere, the hidden information in different MCPCs was revealed and showed distinct color shifts, as shown in Figure 5b. It was conceivable that design of multiple-level implicit images with much more complex responsive properties

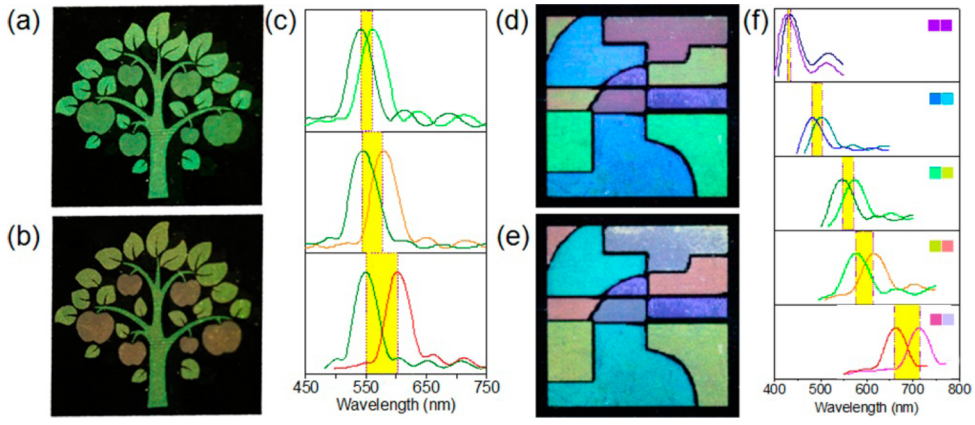

Figure 5. (a and b) Color changes of information hidden MCPC pattern in N_2 and saturated EtOH vapor atmospheres. (c) Reflection spectra of the pattern in N_2 and EtOH vapors. (d and e) Multicolor MCPC pattern in N_2 and saturated EtOH vapor atmospheres. (f) Reflection spectra of the multicolor MCPC pattern in N_2 and EtOH vapors. Each reflection spectrum was marked by colors of corresponing patterns in panels d and e.

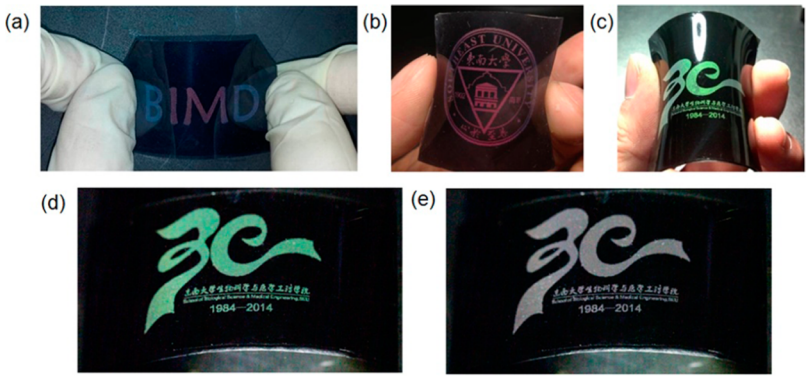

Figure 6. (a) BIMD characters printed on a modified PDMS substrate with a CA of 55°. (b and c) Logos printed on a modified PDMS film with a CA of 90°. (d and e) MCPC pattern in N_2 and EtOH vapors. Logos provided by and used with permission from School of Biological Science and Medical Engineering in Southeast University.

could greatly improve their security levels for anticounterfeiting applications. The reflection spectra of three kinds of CPCs in N_2 and EtOH vapors were plotted in Figure 5c. It was clear that the reflection peak position movements of three CPCs were well controlled. Another multicolor MCPC pattern with complex vapor-responsive color shifting feature was illustrated in Figure 5d,e. The multicolor MCPC pattern was composed of five kinds of MCPCs. These MCPCs displayed distinct color shift extent after exposure to EtOH vapor, as shown in Figure 5f. The complex vapor-responsive color shifting features of the multicolor pattern were easy to recognize by naked eyes for visual authentication but raise the difficulty for counterfeiters to forge, and thus, were of great potential for anticounterfeiting applications.

Angle-Independent Flexible MCPCs Patterns. For practical applications such as anticounterfeit patterns, wearable sensors or displays, construction of responsive CPCs on flexible substrates was of great importance. Herein we also successfully demonstrated the responsive MCPC patterns on flexible substrates. As shown in Figure 6a, a MCPC pattern was printed on flexible polydimethylsiloxane (PDMS) substrate with a contact angle (CA) of 55° (see Supporting Information Figure S8a). The MCPC pattern underwent several times of bending, and owned an angle-dependent structural color. However, the angle-dependent structural color was not favorable for facile dynamic visual authentication when the pattern was curved. By adjusting the wettability of the substrate, we prepared MCPC patterns with angle-independent structural color. As shown in Figure 6b,c, two MCPC patterns were prepared on PDMS films with CA of 90° (see Supporting Information Figure S8b). The structural colors were angle independent; the reflection spectra of MCPC patterns in Figure 6b at different viewing angles were displayed in Supporting Information Figure S9. The results suggested that the reflection peak positions of the logos were almost unchanged at different view angles. This angle independent property of the MCPC pattern was due to the high height/diameter rate of MCPC domes,[42] as seen in Supporting Information Figure S10. When MCPCs domes with high height/diameter rates were at different positions in the viewing field, they reflected the incident light that passed through their centers back. Therefore, the refection peak positions detected were similar. The vapor-chromic authentication of MCPC pattern on curved PDMS substrate was shown in Figure 6d,e. The color change of the MCPC pattern was facile to recognize and did not interfere with view angle when it was exposed to EtOH vapor.

CONCLUSIONS

In summary, we have developed multiple responsive CPC patterns with vapor-revealed implicit images by inkjet printing MSNs inks on rigid or flexible substrates. The vapor-responsive color shifting properties of MCPCs patterns are precisely controlled by design of MSNs in the printing inks. Therefore, multicolor responsive MCPC patterns with vapor-revealed implicit images are subsequently prepared. The complex dynamic vapor-chromic features of multicolor MCPC patterns are reversible and repeatable, easy for naked eye recognition, but hard to copy; thus, they are favorable for anticounterfeiting applications. Moreover, due to the flexible design of inks compositions of inkjet printing, integration of other stimulus-responsive CPCs by this method is of great promise. Therefore, this direct writing patterning technology is also potentially useful for developing novel responsive CPC devices with miniaturization, multiple functions, and convenience.

METHODS

Synthesis of MSNs. SSNs were achieved from Nanjing Dongjian Biological Technology Co., Ltd. MSNs were synthesized by mixing 1.2 g silica spheres, 30 mL of aqueous ammonia (28 wt %), 400 mL of absolute EtOH, 800 mL of deionized water, and 6 mL of cetyltrimethylammonium chloride (C_{16}TACl, 25 wt % in H_2O). After a stirring period of 30 min, tetraethoxysilane (TEOS)

with certain amount was added to the reaction mixture drop by drop, and the solution was subsequently stirred at ambient temperature overnight to achieve a series of MSNs with different mesoporous shell thicknesses. Then, as-synthesized MSNs suspension was centrifuged and dried at 343 K overnight. The resulting dry composite powder was further calcined at 823 K for 6 h in air in order to remove C_{16}TACl.

Preparation of Latex Inks for Printing. Printing inks were prepared by adding 0.5 mL ethylene glycol to a latex suspension (2 mL) containing 20 wt % MSNs or SSNs and then mixing in an ultrasonic bath for 10 min. Then the latex suspension was filtered through a micropore filter with a pore size of 800 nm before use.

Surface Treatment of Substrates. PDMS films were doped with melanin. A plasma cleaner (DT-01, SZ-Omega Ltd., China) was used to make substrates (silicon wafers or PDMS films) hydrophilic. Then, the substrates were placed in a culture dish with 0.5 mL of EtOH solution containing 1 wt % alkoxysilane (triethoxypropylsilane, triethoxyhexylsilane, or triethoxyoctylsilane), and the mixture was heated at 60 °C for 1 h to gain different wettability (CA = 50°, 70°, 90°).

Inkjet Printing MCPC Patterns. MCPC patterns composed of different kinds of CPC microdots were obtained by inkjet printing the corresponding latex ink onto modified substrates with a CA of 60° at room temperature using an Jetlab II tabletop printing platform. Then, the patterns were heated at 35 °C to allow the assembling of nanoparticles. The relative humidity was kept at 40% during the experiments.

Authentications of the MCPC Patterns. The MCPC pattern was placed in a transparent chamber connected with an inlet and outlet. Vapor-chromic features of the security patterns were authenticated by alternately exposing to N_2 and EtOH vapor.

Characterization. Scanning electron microscope (SEM, S-3000N, Hitachi) was used to see the arrangements of the nanoparticles. Field emission scanning electron microscope (FESEM, Zeiss Ultra Plus) was used to obtain the side-view images of the printed dots. Transmission electron microscope (TEM, JEM2100EX) was used to obtain the image of MSNs and SSNs. Reflective spectra were recorded using a fiber optic UV−vis spectrometer (Ocean Optic HR2000CG). CAs were measured using a CA measurement device (Powereach, Zhongchen).

Conflict of Interest: The authors declare no competing financial interest.

Acknowledgment. This work was supported by NSFC (Grant No. 51102043), the Program for Changjiang Scholars and Innovative Research Team in University (IRT1222), Qing Lan Project, 333 Talent Project Foundation of Jiangsu Province and the Science and Technology Development Program of Suzhou (Grant No. SYN201307). The authors thank the School of Biological Science and Medical Engineering in Southeast University for providing the logos in Figure 6 and express our sincere congratulations for its 30th anniversary celebration.

Supporting Information Available: SEM images of the cross section/side view of MCPC microdots, responsive reflection peak shifts of MCPC pattern to different vapors, TEM images of MSNs, photograph of MCPC films, N_2 adsorption/desorption isotherms of MSNs and SSNs, CA of modified substrates, reflection spectra of angle-dependent/independent MCPC patterns at different viewing angles. This material is available free of charge *via* the Internet at http://pubs.acs.org.

REFERENCES AND NOTES

1. Ge, J. P.; Yin, Y. D. Responsive Photonic Crystals. *Angew. Chem., Int. Ed.* **2011**, *50*, 1492–1522.
2. Zhao, Y. J.; Xie, Z. Y.; Gu, H. C.; Zhu, C.; Gu, Z. Z. Bio-Inspired Variable Structural Color Materials. *Chem. Soc. Rev.* **2012**, *41*, 3297–3317.
3. Wang, J. X.; Zhang, Y. Z.; Wang, S. T.; Song, Y. L.; Jiang, L. Bioinspired Colloidal Photonic Crystals with Controllable Wettability. *Acc. Chem. Res.* **2011**, *44*, 405–415.
4. Ueno, K.; Matsubara, K.; Watanabe, M.; Takeoka, Y. An Electro- and Thermochromic Hydrogel as a Full-Color Indicator. *Adv. Mater.* **2007**, *19*, 2807–2812.
5. Kim, H.; Ge, J. P.; Kim, J.; Choi, S.-e.; Lee, H.; Lee, H.; Park, W.; Yin, Y. D.; Kwon, S. Structural Colour Printing Using a Magnetically Tunable and Lithographically Fixable Photonic Crystal. *Nat. Photonics* **2009**, *3*, 534–540.
6. Arsenault, A. C.; Puzzo, D. P.; Manners, I.; Ozin, G. A. Photonic-Crystal Full-Colour Displays. *Nat. Photonics* **2007**, *1*, 468–472.
7. Ge, J. P.; Lee, H.; He, L.; Kim, J.; Lu, Z. D.; Kim, H.; Goebl, J.; Kwon, S.; Yin, Y. D. Magnetochromatic Microspheres Rotating Photonic Crystals. *J. Am. Chem. Soc.* **2009**, *131*, 15687–15694.
8. Fenzl, C.; Hirsch, T.; Wolfbeis, O. S. Photonic Crystals for Chemical Sensing and Biosensing. *Angew. Chem., Int. Ed.* **2014**, *53*, 3318–3335.
9. MacConaghy, K. I.; Geary, C. I.; Kaar, J. L.; Stoykovich, M. P. Photonic Crystal Kinase Biosensor. *J. Am. Chem. Soc.* **2014**, *136*, 6896–6899.
10. Zhao, Y. J.; Zhao, X. W.; Hu, J.; Xu, M.; Zhao, W. J.; Sun, L. G.; Zhu, C.; Xu, H.; Gu, Z. Z. Encoded Porous Beads for Label-Free Multiplex Detection of Tumor Markers. *Adv. Mater.* **2009**, *21*, 569–572.
11. Burgess, I. B.; Mishchenko, L.; Hatton, B. D.; Kolle, M.; Lončar, M.; Aizenberg, J. Encoding Complex Wettability Patterns in Chemically Functionalized 3D Photonic Crystals. *J. Am. Chem. Soc.* **2011**, *133*, 12430–12432.
12. Hou, J.; Zhang, H. C.; Yang, Q.; Li, M. Z.; Song, Y. L.; Jiang, L. Bio-Inspired Photonic-Crystal Microchip for Fluorescent Ultratrace Detection. *Angew. Chem.* **2014**, *126*, 5901–5905.
13. Huang, Y.; Li, F. Y.; Qin, M.; Jiang, L.; Song, Y. L. A Multi-Stopband Photonic-Crystal Microchip for High-Performance Metal-Ion Recognition Based on Fluorescent Detection. *Angew. Chem.* **2013**, *125*, 7437–7440.
14. Arsenault, A. C.; Clark, T. J.; Von Freymann, G.; Cademartiri, L.; Sapienza, R.; Bertolotti, J.; Vekris, E.; Wong, S.; Kitaev, V.; Manners, I.; *et al.* From Colour Fingerprinting to the Control of Photoluminescence in Elastic Photonic Crystals. *Nat. Mater.* **2006**, *5*, 179–184.
15. Furumi, S.; Kanai, T.; Sawada, T. Widely Tunable Lasing in a Colloidal Crystal Gel Film Permanently Stabilized by an Ionic Liquid. *Adv. Mater.* **2011**, *23*, 3815–3820.
16. Hu, H. B.; Zhong, H.; Chen, C. L.; Chen, Q. W. Magnetically Responsive Photonic Watermarks on Banknotes. *J. Mater. Chem. C* **2014**, *2*, 3695–3702.
17. Lee, H. S.; Shim, T. S.; Hwang, H.; Yang, S.-M.; Kim, S.-H. Colloidal Photonic Crystals toward Structural Color Palettes for Security Materials. *Chem. Mater.* **2013**, *25*, 2684–2690.
18. Xuan, R. Y.; Ge, J. P. Invisible Photonic Prints Shown by Water. *J. Mater. Chem.* **2012**, *22*, 367–372.
19. Hu, H. B.; Chen, Q. W.; Tang, J.; Hu, X. Y.; Zhou, X. H. Photonic Anti-Counterfeiting Using Structural Colors Derived from Magnetic-Responsive Photonic Crystals with Double Photonic Bandgap Heterostructures. *J. Mater. Chem.* **2012**, *22*, 11048–11053.
20. Ding, T.; Luo, L.; Wang, H.; Chen, L.; Liang, K.; Clays, K.; Song, K.; Yang, G.; Tung, C.-H. Patterning and Pixelation of Colloidal Photonic Crystals for Addressable Integrated Photonics. *J. Mater. Chem.* **2011**, *21*, 11330–11334.
21. Lee, S. K.; Yi, G. R.; Moon, J. H.; Yang, S. M.; Pine, D. J. Pixellated Photonic Crystal Films by Selective Photopolymerization. *Adv. Mater.* **2006**, *18*, 2111–2116.
22. Zhang, J. H.; Yang, B. Patterning Colloidal Crystals and Nanostructure Arrays by Soft Lithography. *Adv. Funct. Mater.* **2010**, *20*, 3411–3424.
23. Kim, T.-H.; Cho, K.-S.; Lee, E. K.; Lee, S. J.; Chae, J.; Kim, J. W.; Kim, D. H.; Kwon, J.-Y.; Amaratunga, G.; Lee, S. Y.; *et al.* Full-Colour Quantum Dot Displays Fabricated by Transfer Printing. *Nat. Photonics* **2011**, *5*, 176–182.
24. Ge, J. P.; Goebl, J.; He, L.; Lu, Z. D.; Yin, Y. D. Rewritable Photonic Paper with Hygroscopic Salt Solution as Ink. *Adv. Mater.* **2009**, *21*, 4259–4264.
25. Ozin, G. A.; Arsenault, A. C. P-Ink and Elast-Ink from Lab to Market. *Mater. Today* **2008**, *11*, 44–51.
26. Fudouzi, H.; Xia, Y. N. Photonic Papers and Inks: Color Writing with Colorless Materials. *Adv. Mater.* **2003**, *15*, 892–896.

27. Shim, T. S.; Kim, S.-H.; Sim, J. Y.; Lim, J.-M.; Yang, S.-M. Dynamic Modulation of Photonic Bandgaps in Crystalline Colloidal Arrays Under Electric Field. *Adv. Mater.* **2010**, *22*, 4494–4498.
28. Singh, M.; Haverinen, H. M.; Dhagat, P.; Jabbour, G. E. Inkjet Printing—Process and Its Applications. *Adv. Mater.* **2010**, *22*, 673–685.
29. Minemawari, H.; Yamada, T.; Matsui, H.; Tsutsumi, J. Y.; Haas, S.; Chiba, R.; Kumai, R.; Hasegawa, T. Inkjet Printing of Single-Crystal Films. *Nature* **2011**, *475*, 364–367.
30. Torrisi, F.; Hasan, T.; Wu, W. P.; Sun, Z. P.; Lombardo, A.; Kulmala, T. S.; Hsieh, G.-W.; Jung, S. J.; Bonaccorso, F.; Paul, P. J.; *et al.* Inkjet-Printed Graphene Electronics. *ACS Nano* **2012**, *6*, 2992–3006.
31. James, D. T.; Kjellander, B. K. C.; Smaal, W. T. T.; Gelinck, G. H.; Combe, C.; McCulloch, I.; Wilson, R.; Burroughes, J. H.; Bradley, D. D. C.; Kim, J.-S. Thin-Film Morphology of Inkjet-Printed Single-Droplet Organic Transistors Using Polarized Raman Spectroscopy Effect of Blending TIPS-Pentacene with Insulating Polymer. *ACS Nano* **2011**, *5*, 9824–9835.
32. Li, J. T.; Ye, F.; Vaziri, S.; Muhammed, M.; Lemme, M. C.; Östling, M. Efficient Inkjet Printing of Graphene. *Adv. Mater.* **2013**, *25*, 3985–3992.
33. Dasgupta, S.; Kruk, R.; Mechau, N.; Hahn, H. Inkjet Printed, High Mobility Inorganic-Oxide Field Effect Transistors Processed at Room Temperature. *ACS Nano* **2011**, *5*, 9628–9638.
34. Wang, J. X.; Wang, L. B.; Song, Y. L.; Jiang, L. Patterned Photonic Crystals Fabricated by Inkjet Printing. *J. Mater. Chem. C* **2013**, *1*, 6048–6058.
35. Kuang, M. X.; Wang, L. B.; Song, Y. L. Controllable Printing Droplets for High-Resolution Patterns. *Adv. Mater.* **2014**, 10.1002/adma.201305416.
36. Shen, W. Z.; Li, M. Z.; Ye, C. Q.; Jiang, L.; Song, Y. L. Direct-Writing Colloidal Photonic Crystal Microfluidic Chips by Inkjet Printing for Label-Free Protein Detection. *Lab Chip* **2012**, *12*, 3089–3095.
37. Ko, H.-Y.; Park, J. H.; Shin, H. J.; Moon, J. Rapid Self-Assembly of Monodisperse Colloidal Spheres in an Ink-Jet Printed Droplet. *Chem. Mater.* **2004**, *16*, 4212–4215.
38. Park, J. H.; Moon, J. H. Control of Colloidal Particle Deposit Patterns within Picoliter Droplets Ejected by Ink-Jet Printing. *Langmuir* **2006**, *22*, 3506–3513.
39. Sele, C. W.; Werne, T. V.; Friend, R. H.; Sirringhaus, H. Lithography-Free, Self-Aligned Inkjet Printing with Sub-Hundred-Nanometer Resolution. *Adv. Mater.* **2005**, *17*, 997–1001.
40. Chu, K.-H.; Xiao, R.; Wang, E. N. Uni-Directional Liquid Spreading on Asymmetric Nanostructured Surfaces. *Nat. Mater.* **2010**, *9*, 413–417.
41. Cui, L. Y.; Li, Y. F.; Wang, J. X.; Tian, E. T.; Zhang, X. Y.; Zhang, Y. Z.; Song, Y. L.; Jiang, L. Fabrication of Large-Area Patterned Photonic Crystals by Ink-Jet Printing. *J. Mater. Chem.* **2009**, *19*, 5499–5502.
42. Kuang, M. X.; Wang, J. X.; Bao, B.; Li, F. Y.; Wang, L. B.; Jiang, L.; Song, Y. L. Inkjet Printing Patterned Photonic Crystal Domes for Wide Viewing-Angle Displays by Controlling the Sliding Three Phase Contact Line. *Adv. Optical Mater.* **2014**, *2*, 34–38.
43. Liu, F.; Dong, B. Q.; Liu, X. H.; Zheng, Y. M.; Zi, J. Structural Color Change in Longhorn Beetles Tmesisternus Isabellae. *Opt. Express* **2009**, *17*, 16183–16191.
44. Wagner, T.; Haffer, S.; Weinberger, C.; Klaus, D.; Tiemann, M. Mesoporous Materials as Gas Sensors. *Chem. Soc. Rev.* **2013**, *42*, 4036–4053.
45. Wu, Z. X.; Zhao, D. Y. Ordered Mesoporous Materials as Adsorbents. *Chem. Commun.* **2011**, *47*, 3332–3338.
46. Colodrero, S.; Ocana, M.; Gonzalez-Elipe, A. R.; Miguez, H. Response of Nanoparticle-based One-Dimensional Photonic Crystals to Ambient Vapor Pressure. *Langmuir* **2008**, *24*, 9135–9139.
47. Kelly, T. L.; Garcia Sega, A.; Sailor, M. J. Identification and Quantification of Organic Vapors by Time-Resolved Diffusion in Stacked Mesoporous Photonic Crystals. *Nano Lett.* **2011**, *11*, 3169–3173.
48. Yamada, Y.; Nakamura, T.; Ishi, M.; Yano, K. Reversible Control of Light Reflection of a Colloidal Crystal Film Fabricated From Monodisperse Mesoporous Silica Spheres. *Langmuir* **2006**, *22*, 2444–2446.
49. Bonifacio, L. D.; Puzzo, D. P.; Breslav, S.; Willey, B. M.; McGeer, A.; Ozin, G. A. Towards the Photonic Nose a Novel Platform for Molecule and Bacteria Identification. *Adv. Mater.* **2010**, *22*, 1351–1354.
50. Xie, Z. Y.; Cao, K. D.; Zhao, Y. J.; Bai, L.; Gu, H. C.; Xu, H.; Gu, Z. Z. An Optical Nose Chip Based on Mesoporous Colloidal Photonic Crystal Beads. *Adv. Mater.* **2014**, *26*, 2413–2418.
51. Kobler, J.; Lotsch, B. V.; Ozin, G. A.; Bein, T. Vapor-Sensitive Bragg Mirrors and Optical Isotherms from Mesoporous Nanoparticle Suspensions. *ACS Nano* **2009**, *3*, 1669–1676.